Exploring hidden sectors with two-particle angular correlations at future e^+e^- colliders

E. Musumeci[1]**, A. Irles**[a,1]**, R. Perez-Ramos** [2,3]**, I. Corredoira**[4]**,
E. Sarkisyan-Grinbaum**[5,6]**, V. A. Mitsou**[1]**, M. A. Sanchis-Lozano**[1]

[1]IFIC, Universitat de València and CSIC, C./ Catedrático José Beltrán 2, E-46980 Paterna, Spain

[2]DRII-IPSA, 63 bis Boulevard de Brandebourg, 94200 Ivry-sur-Seine, France

[3]Laboratoire de Physique Théorique et Hautes Energies (LPTHE), UMR 7589, Sorbonne Université et CNRS, 4 place Jussieu, 75252 Paris Cedex 05, France

[4]Instituto Galego de Física de Altas Enerxìas (IGFAE, USC), Spain

[5]Experimental Physics Department, CERN, 1211 Geneva 23, Switzerland

[6]Department of Physics, The University of Texas at Arlington, Arlington, TX 76019, USA

Abstract Future e^+e^- colliders are called to play a fundamental role in measuring Standard Model (SM) parameters with unprecedented precision and the discovery of physics beyond the SM (BSM). This study focus on a QCD-like Hidden Valley (HV) scenario, with relatively light v-quarks ($\lesssim 100$ GeV), perturbing the QCD partonic cascade and modifying azimuthal and (pseudo)rapidity correlations of final-state SM hadrons. Using PYTHIA8 and detector fast simulation tools we study unexpected structures arising in the two-particle angular correlation function, including selection cuts and detector effects.

Keywords e^+e^- colliders, angular correlations, New Physics, Hidden Valley

1 Introduction

Correlations play a fundamental role in the study of hadronic dynamics since the beginning of cosmic ray and accelerator physics [1, 2]. Recently, the study of angular correlations have revealed a new phenomenon in heavy-ion collisions, later also found in smaller system (proton–proton, proton–nucleus) collisions [3–5].

In particular, long-range near-side ridges show up in two-particle angular correlations, while different theoretical explanations have been put forward to understand this initially unexpected phenomenon [6–11]. Almost all of them require the existence of some unconventional state of matter at the primary interaction of the collision (like quark-gluon plasma), ultimately yielding collective effects among final-state SM particles. On the other hand, no clear ridge-like signal was found in the e^+e^- data analysed by ALEPH [12] and Belle [13] experiments, except for recent claims in [14] at the highest available energy and high multiplicity of the former.

Motivated by such unexpected correlation structures found in high-energy collisions, in this work we look at possible *anomalies* (not only ridge effects) in both azimuthal and (pseudo)rapidity correlations to obtain a useful insight into an unknown stage of matter on top of the QCD parton shower. We focus on two-particle angular correlations as a way of searching for BSM at future high-energy e^+e^- colliders, as they provide a much cleaner environment than hadron colliders. The theoretical framework of New Physics (NP) used in this work is based on the so-called *Hidden Valley* (HV) scenario, which stands for a wide class of models with one or more hidden sectors beyond the SM. Thereby, new (valley) particles of mass $\lesssim 100$ GeV arise, still surviving all present discovery limits.

2 Two-particle angular correlations

The clean environment of e^+e^- collisions, in contrast to hadronic collisions, is especially suitable to define a reference frame whose z-axis lies along the direction of the back-to-back jets in most events. The thrust reference frame has been used throughout this work, so the rapidity y of a particle always refers to the thrust or z-axis. The azimuthal angle ϕ is defined as usual on the transverse plane to the thrust axis, event by event. Note that only rapidity and azimuthal differences of two final-state SM charged particles labelled as '1' and '2', $\Delta y \equiv y_1 - y_2$, $\Delta\phi \equiv \phi_1 - \phi_2$, will be used in our study.

---

[a]Corresponding author

The two-particle correlation function is defined as

$$C^{(2)}(\Delta y, \Delta \phi) = \frac{S(\Delta y, \Delta \phi)}{B(\Delta y, \Delta \phi)}, \tag{1}$$

where $S(\Delta y, \Delta \phi)$ stands for the density of particle pairs within the same event

$$S(\Delta y, \Delta \phi) = \frac{1}{N_{\text{pairs}}} \frac{d^2 N^{\text{same}}}{d\Delta y d\Delta \phi}, \tag{2}$$

while $B(\Delta y, \Delta \phi)$ represents the density of mixed particle pairs from distinct events

$$B(\Delta y, \Delta \phi) = \frac{1}{N_{\text{mix}}} \frac{d^2 N^{\text{mix}}}{d\Delta y d\Delta \phi}. \tag{3}$$

The so-called azimuthal yield, $Y(\Delta \phi)$, is of particular interest, being defined by integration over a given Δy range as:

$$Y(\Delta \phi) = \frac{\int_{y_{\text{inf}} \leq |\Delta y| \leq y_{\text{sup}}} S(\Delta y, \Delta \phi) dy}{\int_{y_{\text{inf}} \leq |\Delta y| \leq y_{\text{sup}}} B(\Delta y, \Delta \phi) dy}, \tag{4}$$

where $y_{\text{inf/sup}}$ defines the lower/upper integration limit for different rapidity intervals.

3 HV phenomenology

In most HV models [15], the SM gauge group sector G_{SM} is extended by (at least) a new gauge group G_{V} under which all SM particles are neutral. Hence, a new category of *v-particles* emerges charged under G_{V}, but neutral under G_{SM}. Moreover, "communicators", charged under both G_{SM} and G_{V}, are introduced to the theory allowing interactions between SM and HV particles. Communicators can be either intermediate (very massive) vector Z_v bosons, or hidden partners of SM quarks or leptons, generically denoted as F_v, assumed to be pair produced. In this study, F_v are taken as fermions (spin = 1/2) and q_v scalars.

Different mechanisms can connect the hidden and SM sectors through communicators, e.g., via the tree-level channel: $e^+ e^- \rightarrow Z_v \rightarrow q_v \bar{q}_v \rightarrow$ hadrons. Alternatively, communicators can be pair produced via SM γ^*/Z coupling to a $F_v \bar{F}_v$ pair, yielding both visible and invisible cascades in the same event. We have checked that the latter channel significantly dominates over the former within the range of energies under study.

For some values of the HV parameter space, communicators can *promptly* decay into a particle f of the visible sector (its SM partner) and a q_v of the hidden sector according to the splitting: $F_v \rightarrow f q_v$. Note that the q_v mass may strongly influence the kinematics of the visible cascade (leading to SM particles) in the same event,
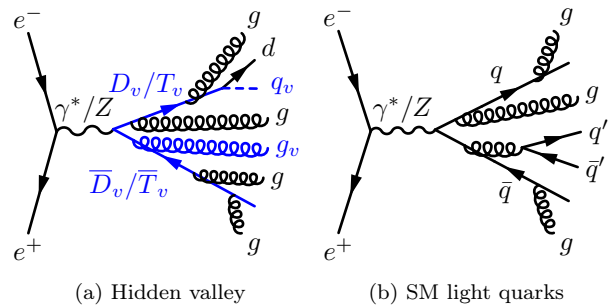

(a) Hidden valley   (b) SM light quarks

Fig. 1: Leading diagrams of production in $e^+ e^-$ collisions for (a) HV, and (b) SM light quarks including bottom.

thereby yielding observational consequences. This mass remains currently unconstrained ranging from zero to close to the F_v mass [16], so that different values of it will be assumed in our analysis.

Indeed, we are especially interested in the influence of the invisible (HV) sector on the partonic cascade into final-state SM particles, leading to potentially observable effects. This can be understood, e.g., as both visible and hidden cascades have to share the event's total energy, thereby modifying their respective available phase spaces. For the sake of concreteness, we restrict our study to a QCD-like HV scenario with q_v-quarks, g_v-gluons, and an equivalent "strong" coupling constant α_v. For simplicity, α_v is assumed not running with energy but fixed to $\alpha_v = 0.1$, as no significant differences were found in our analysis by varying this value.

4 Analysis at detector level

To assess the feasibility of HV signal detection in $e^+ e^-$ colliders, we have relied throughout on the PYTHIA8 Monte Carlo event generator [17] because of its firmly established reliability and the fact that the HV production channel is already built in. Fast detector simulations were performed using the SGV tool [18] and the geometry and acceptances corresponding to the large model of the ILD concept for the International Linear Collider (ILC) as described in [19]. The simulated events are provided in the same event model as used by the ILD concept group, and the tools available in the ILCSOFT package are used for the event reconstruction and analysis. The ILD reconstruction is based on the so-called Particle Flow approach, which aims to reconstruct all individual particles produced in the final state via pattern recognition algorithms. The reconstructed candidates of single particles are called Particle Flow Objects (PFOs). In our study, including de-

tector effects, we set the centre-of-mass energy $\sqrt{s}$ of e^+e^- collisions equal to 250 GeV to coincide with the planned first commissioning of the collider as a Higgs boson factory. As a further outlook, we extended our prospective study (this time only at particle level) up to $\sqrt{s} = 500$ GeV and 1 TeV. The case of longitudinally polarised beams will be addressed in a future work once this option becomes available.

As already commented in the previous section, the HV signal proceeds via the process $e^+e^- \to D_v \bar{D}_v \to$ hadrons (where D_v denotes the lightest communicator, being the hidden partner of the d-quark) as depicted in Fig. 1a. In our benchmark scenarios we set $\alpha_v = 0.1$, $m_{D_v} = 125$ GeV, with four different v-quark mass values: $m_{q_v} = 0.1, 10, 50$ and 100 GeV. We also consider $m_{D_v} = 80$ and 100 GeV with $m_{q_v} = 40$ and 50 GeV respectively. At higher $\sqrt{s}$, we also included $T_v \bar{T}_v$ pair production assuming that it becomes kinematically possible.

In our analysis at $\sqrt{s} = 250$ GeV, the $e^+e^- \to q\bar{q}$ background comes from the inclusive production of all the SM quark species except the top flavour, since its production lies below threshold (see Fig. 1).

In a preceding investigation [20], the aforementioned signal and background were examined at particle level. Besides, no Initial State Radiation (ISR) was included although it plays a crucial role in the analysis, as we shall see soon. Four-fermion production (dominated by $e^+e^- \to WW$) was neither considered but its contribution has been found to be negligible. In the present work, we broaden our study to detector level taking into account the ISR effect. The cross-sections for the HV and SM processes have been estimated from PYTHIA8 reported in Table 1.

In view of the small cross-sections for HV production from Table 1, specific cuts have to be implemented to maximise the background removal while keeping the signal as much as possible. On the other hand, displaced vertices due to the production and decay of long-lived particles have not been considered here as we are focusing on prompt decays of v-particles and their effect on the partonic cascade yielding final-state SM particles. Following similar strategy as in [21], constraints have been set on the number of neutral PFOs and charged ones (≤ 22 and ≤ 15, respectively). Other cuts were applied to the emission angle ($|\cos\theta_{\gamma_{\mathrm{ISR}}}| < 0.5$) and energy ($E_{\gamma_{\mathrm{ISR}}} < 40$ GeV) of reconstructed ISR photons. Constraints on the di-jet invariant mass m_{jj} have also been defined, accepting values below 130 GeV. Furthermore, an energy upper limit of 80 GeV was implemented to the leading jet.

The selection-cut efficiency, reported in Table 1, shows a drastic reduction of the SM background while the HV

Table 1: Cross-sections for $e^+e^- \to D_v\bar{D}_v$, $e^+e^- \to q\bar{q}$ and $WW \to 4q$ processes at $\sqrt{s} = 250$ GeV, with different assignments for the m_{D_v} and m_{q_v} masses. Efficiencies of the selection criteria described in the main text, average charged-track multiplicities and their RMS, are shown.

| Process		$\sigma_{\mathrm{PYTHIA8}}$ [pb]	Efficiency [%]	$\langle N_{\mathrm{ch}} \rangle$
$e^+e^- \to D_v\bar{D}_v$	m_{D_v}			
$m_{q_v} = 0.1$ GeV	125 GeV	0.13	36	12.4±3.7
$m_{q_v} = 10$ GeV	125 GeV	0.12	36	12.4±3.7
$m_{q_v} = 50$ GeV	125 GeV	0.12	42	11.4±3.5
$m_{q_v} = 100$ GeV	125 GeV	0.12	42	6.5±2.1
$m_{q_v} = 50$ GeV	100 GeV	1.29	42	11.1±3.4
$m_{q_v} = 40$ GeV	80 GeV	1.54	36	18.0±4.9
$e^+e^- \to q\bar{q}$ with ISR		48	$\lesssim 0.01$	9.9±3.4
$WW \to 4q$		7.4	$\lesssim 0.001$	–

signal is affected to a much lesser extent. For the computation of B, only a thrust value larger than 0.95 was imposed, keeping the same requirements on PFO multiplicities as for S.

Figure 2 shows three-dimensional plots of the two-particle correlation function $C^{(2)}(\Delta y, \Delta\phi)$ separately for the HV and SM scenarios, before (Fig. 2a) and after (Fig. 2b) cuts. As a reference example, in the HV case we set $m_{q_v} = 100$ GeV, $m_{D_v} = 125$ GeV and $\alpha_v = 0.1$ alongside the decay $D_v \to d + q_v$ initiating the partonic (both visible and invisible) shower. As expected, a near-side peak shows up at ($\Delta y \simeq 0$, $\Delta\phi \simeq 0$), receiving contributions mainly from track pairs within the same jet. On the other hand, an away-side correlation ridge around $\Delta\phi \simeq \pi$, and extending over a large rapidity range, results from back-to-back momentum balance, in principle unrelated to NP effects. After cuts, a near-side ridge (with two pronounced and symmetric bumps) shows up for $1.6 < |\Delta y| < 3$ at $\Delta\phi \simeq 0$ for the SM case, similar to the pure HV scenario. This structure arises from the ISR effect, since the effective center-of-mass energy approaches the Z mass, and thus resonant production greatly enhances the production cross-section. It becomes of paramount importance to take this effect into account in our analysis, mimicking possible HV signatures in angular correlations.

In order to examine in more detail the possibility of discriminating the HV signal from the pure SM background, we depict in Fig. 3 the yield $Y(\Delta\phi)$ (defined in Eq. (4)) for both $0 < |\Delta y| \leq 1.6$ and $1.6 < |\Delta y| < 5$ ranges: before (Fig. 3a) and after (Fig. 3b) cuts. Note that the HV signal for various masses m_{D_v}, m_{q_v} is considered together with the SM background, while a stan-
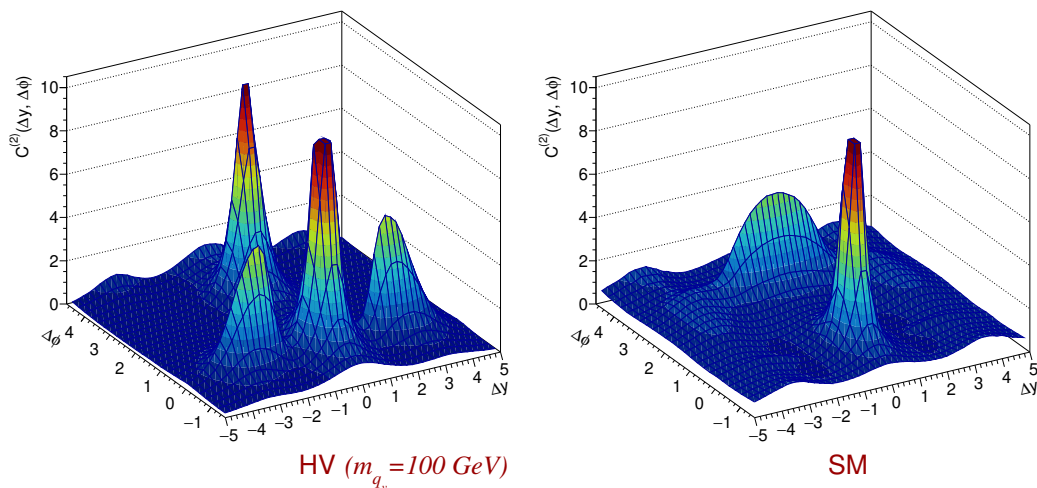
(a) Detector level distributions with no selection applied to the $S(\Delta y, \Delta \phi)$ reconstruction.
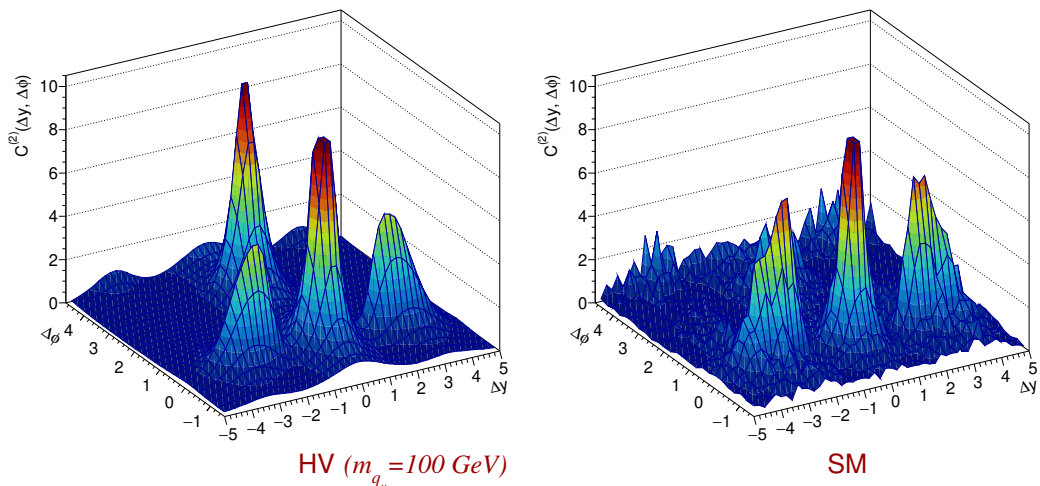
(b) Detector level distributions after the signal enriching experimental cuts applied to the $S(\Delta y, \Delta \phi)$ reconstruction.

Fig. 2: 3D plots of the two-particle angular correlation function, $C^{(2)}(\Delta y, \Delta \phi)$, at detector level, separately for the pure HV signal and the SM background in e^+e^- collisions at $\sqrt{s} = 250$ GeV. In the pure HV case, $m_{q_v} = 100$ GeV, $m_{D_v} = 125$ GeV and $\alpha_v = 0.1$ were set. For the SM case, light quarks include the bottom flavour.

dalone analysis of the SM background is also presented. A clear difference becomes apparent for $0 < |\Delta y| \leq 1.6$: a sizeable peak at $\Delta \phi \sim \pi$ characterises the HV scenario, unlike the pure SM case. This remarkable discrepancy of shapes would potentially serve as a valuable signature of a hidden sector, complementary to more conventional BSM searches, as claimed in this study.

5 Prospects on the experimental sensitivity

Let us stress that an analysis to search for BSM physics in high-energy collisions relying on angular correlations

(as proposed in this paper) offers several advantages with respect to more conventional methods, e.g., based on an excess of events in cross sections or invariant mass peaks. In particular, yield distributions as defined in Eq.(4) benefit from an almost total cancellation of reconstruction efficiencies and detector acceptances, luminosity and cross-section dependence, etc. However, modelling uncertainties could be a limiting factor for these observables. In order to better understand this issue, we performed a study assuming different scenarios for the foreseen statistic and systematic uncertainties.

To estimate the statistical uncertainties, we assume a collected luminosity of 100 fb^{-1}, which roughly cor-
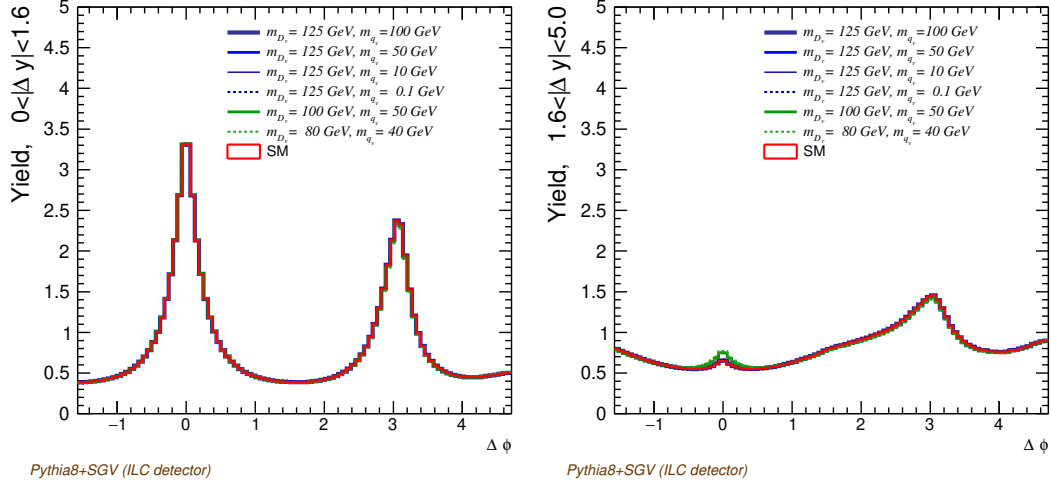
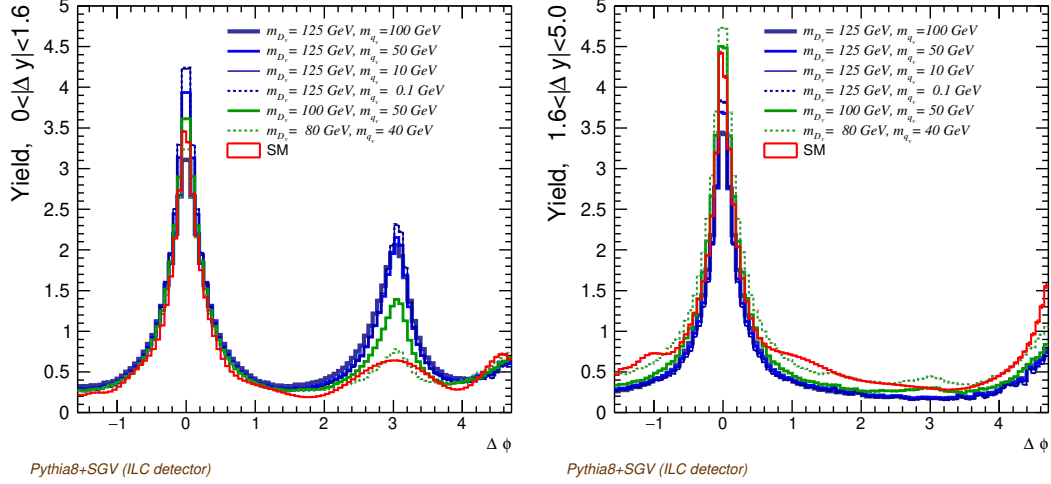(a) Detector-level yield distributions with no selection cuts applied.

(b) Detector-level yield distributions after the selection cuts were applied to enrich the $S(\Delta y, \Delta \phi)$ sample with HV signal events.

Fig. 3: Yield $Y(\Delta \phi)$ for both HV signal in association with SM and for pure SM background (red line) for the $0 < |\Delta y| < 1.6$ (left) and $1.6 < |\Delta y| < 5$ intervals (right), respectively. Notice the different shapes of the HV+SM signal and SM background resulting after applying the selection cuts, providing a valuable signature of NP using angular correlations.

responds to one year of data taking of ILC in the H20-staged scenario [22]. For the systematic uncertainties, we identified two potential main sources: the detector performance modelling and the fragmentation (pertaining to the final hadronisation of the partonic cascade) uncertainties. For both of them, only educated guesses based on current knowledge can be made. For instance, the detector performance modelling uncertainty is evaluated by a bin-by-bin comparison of the estimated yield distributions at particle and detector levels. The absolute value of the difference is taken as uncertainty. This comparison should account for the kinematic reso-

lution (including angular) on the track reconstruction, as well as acceptance effects. We stress that this approach highly overestimates the experimental uncertainties, therefore, it represents a worst-case scenario. For the fragmentation uncertainty, we follow the same recipe as for the detector-effects modelling, but this time we compare the predictions of the yield at the particle level calculated using two different fragmentation models implemented in PYTHIA8 and HERWIG 7.3 [23, 24], respectively. The total uncertainty, calculated also bin by bin, is composed of the addition in quadrature of the statistical uncertainty for the ex-

pected number of events, and the systematic uncertainties of Y_{SM} since only Pythia8 includes Hidden Valley production. The outcome of these assumptions is summarised in Fig. 4, with σ_Y representing the estimated uncertainty as explained above.

Once all the above points are taken into account, it is straightforward to calculate the sensitivity of the observable by comparing the HV and SM predictions for Y with the expected uncertainties. Already at 100 fb^{-1}, the sensitivity is mostly limited by systematic uncertainties as the detector performance systematics is dominant over all the others. However, the discovery power remains almost intact, especially near the sizeable Y peak at $\Delta\phi \sim \pi$ with $0 < |\Delta y| \leq 1.6$. As an exercise, we compare the estimated sensitivity with a much more optimistic scenario in which we improve our knowledge of systematic uncertainties by one order of magnitude with respect to the current estimates assuming a significant improvement in detector-performance-related uncertainties. Dedicated studies on the fragmentation modelling of HV processes would also be required for further understanding. Assuming this order of magnitude improvement, the sensitivity would be drastically enhanced, and the discovery power would be reached for most of the phase space available. Of course, we emphasise that this is only an educated guess that should serve as yet another motivation to pursue the best possible design of future collider detectors and progress on Monte Carlo tools development to minimise modelling uncertainties.

6 Outlook at higher-energies

Till now, we have focused on a future e^+e^- collider operating at $\sqrt{s} = 250$ GeV, but likely those machines will later run at higher energies. Therefore we have extended our study to $\sqrt{s} = 0.5$ and 1 TeV, at particle level for the time being.

As the HV signal $e^+e^- \to Q_v\bar{Q}_v \to$ hadrons, we consider the two extreme cases: the lightest communicator D_v and the heaviest one T_v which decays into $q_v t$. We have confirmed that intermediate masses yield intermediate results. Besides the $q\bar{q}$ and $WW \to 4q$ backgrounds, we also take into account the production of $t\bar{t}$, which, in fact, becomes relevant at these energies. Table 2 presents the cross-sections obtained from Pythia8. We set the mass of D_v and T_v equal to $\sqrt{s}/2$, and results for different m_{q_v} are shown. No large variations are obtained around this mass assignment to the communicator. According to expectations, the contribution from the SM backgrounds decreases with energy. For the HV signal, a reduction of the cross-section by two orders of magnitude is obtained at $\sqrt{s} = 1$ TeV.

Table 2: Cross-sections of the HV signal and SM background at $\sqrt{s} = 500$ GeV and $\sqrt{s} = 1$ TeV. Cross-section predictions do not depend on the m_{q_v} value unless it is too large to make the process kinematically inaccessible. The signal corresponds to D_v and T_v pair production with the D_v/T_v mass set equal to $\sqrt{s}/2$. Whenever kinematically allowed, $t\bar{t}$ production has been included as a SM background source in addition to lighter flavours considered at $\sqrt{s} = 250$ GeV.

| Process	$\sigma_{\sqrt{s}=500\text{GeV}}$ [pb]	$\sigma_{\sqrt{s}=1\text{TeV}}$ [pb]
$e^+e^- \to D_v\bar{D}_v$	$m_{D_v} = 250$ GeV 2.4×10^{-2}	$m_{D_v} = 500$ GeV 4.4×10^{-3}
$e^+e^- \to T_v\bar{T}_v$	$m_{T_v} = 250$ GeV 9.5×10^{-2}	$m_{T_v} = 500$ GeV 1.8×10^{-2}
$e^+e^- \to q\bar{q}$ with ISR	11	2.9
$e^+e^- \to t\bar{t}$	0.59	0.19
$WW \to 4q$	3.4	1.3

7 Conclusions

The analysis of particle correlations in high-energy colliders can provide valuable insights into matter under extreme temperature and density conditions, somehow reproducing the early-universe conditions when quarks and gluons had not yet bound to form hadrons. On the other hand, this kind of analysis can become a complementary tool to other conventional searches to uncover the existence of new phenomena including BSM physics as postulated in Refs. [25, 26] and studied in this work.

Motivated by the experimental observation of unexpected structures shown in angular correlations from hadronic collisions, we have explored at detector level the discovery potential for hidden sectors at future e^+e^- colliders using two-particle angular correlations. Specifically, we consider a QCD-like HV model containing not-too-heavy v-quarks and v-gluons, which can interact with the SM sector via communicators of mass typically $\lesssim 1$ TeV. We have focused on $D_v\bar{D}_v$ pair production at $\sqrt{s} = 250$ GeV, of the order of the expected mass for the lightest communicator in this scenario. We have shortly extended our study at particle level to higher energies (up to 1 TeV), pointing out promising prospects too.

To conclude, our results show that two-particle azimuthal correlations in a e^+e^- Higgs factory could indeed become a useful tool to discover NP if kinematically accessible. Although a specific HV model has been employed, other types of hidden sectors would expectedly yield similar signatures. In addition, collective effects stemming from a source different from BSM cannot be excluded in this kind of analysis. Such searches,
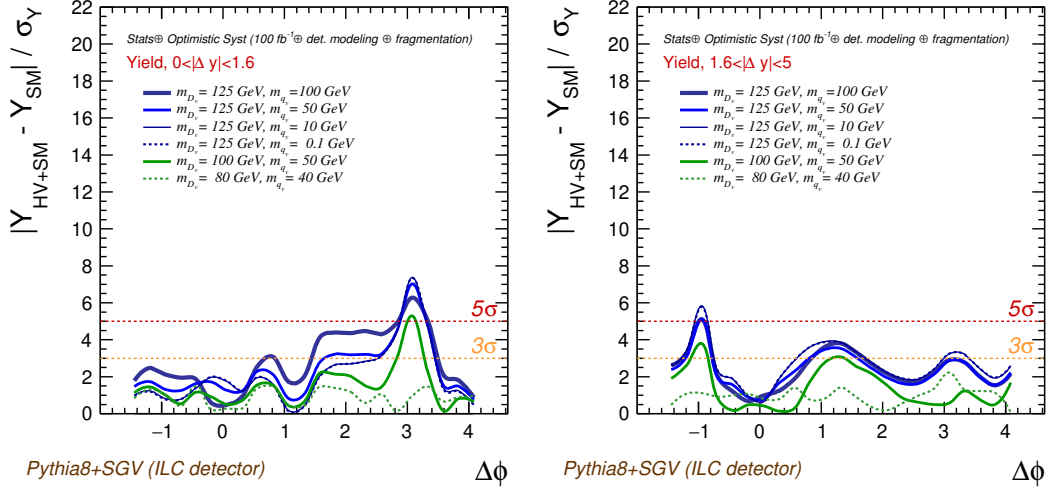
(a) With systematic modelling uncertainties obtained from current state of the art.
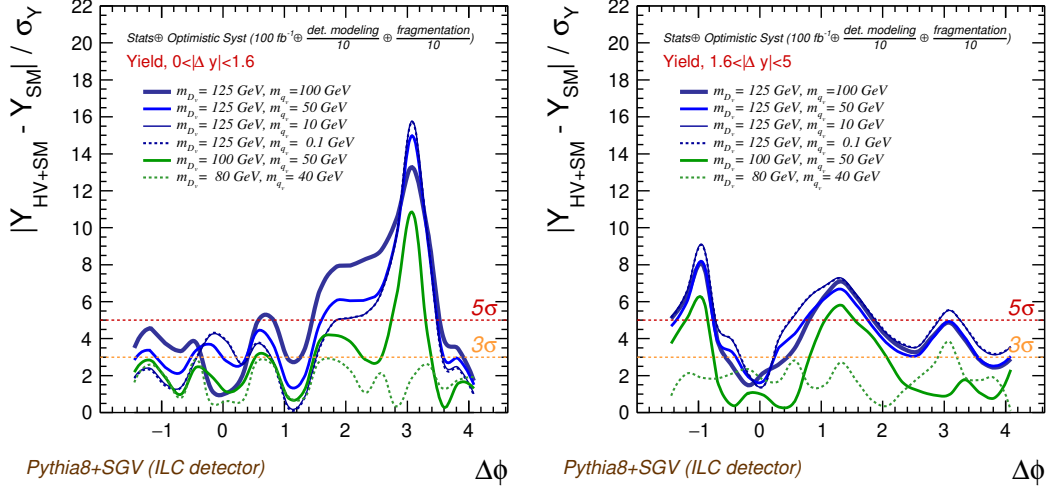
(b) Same as above but assuming an improvement of one order magnitude on the modelling uncertainties evaluation.

Fig. 4: Expected experimental sensitivity for Hidden Valley models along with the SM background after collecting $100 \ \text{fb}^{-1}$ of integrated luminosity, for yield measurements in the range of $0 < |\Delta y| < 1.6$ (left) and $1.6 < |\Delta y| < 5$. (right). The experimental sensitivity is expected to be dominated by systematic uncertainties associated with the detector response and parton shower and fragmentation modelling.

based on rather diffuse signals that spread over a large number of final-state particles, should be contemplated as complementary to other more conventional methods, thereby increasing the discovery potential of these machines.

References

1. W. Kittel and E. A. De Wolf, *Soft multihadron dynamics.* World Scientific, 2005, 10.1142/5805.

2. R. Botet and M. Ploszajczak, *Universal fluctuations: The phenomenology of hadronic matter.* World Scientific, 2002, 10.1142/4916.

3. CMS collaboration, *Measurement of long-range near-side two-particle angular correlations in pp collisions at $\sqrt{s}$ =13 TeV, Phys. Rev. Lett.* **116** (2016) 172302 [1510.03068].

4. ALICE collaboration, *Long-range angular correlations on the near and away side in p-Pb collisions at $\sqrt{s_{NN}}$ = 5.02 TeV, Phys. Lett. B* **719** (2013) 29 [1212.2001].

5. ATLAS collaboration, *Observation of Associated Near-Side and Away-Side Long-Range Correlations in $\sqrt{s_{NN}}$ = 5.02 TeV Proton-Lead Collisions with the ATLAS Detector, Phys. Rev. Lett.* **110** (2013) 182302 [1212.5198].

6. E. V. Shuryak, *On the origin of the 'Ridge' phenomenon induced by jets in heavy ion collisions, Phys. Rev. C* **76** (2007) 047901 [0706.3531].

7. A. Dumitru, F. Gelis, L. McLerran and R. Venugopalan, *Glasma flux tubes and the near side ridge phenomenon at RHIC, Nucl. Phys. A* **810** (2008) 91 [0804.3858].

8. P. Bozek and W. Broniowski, *Collective dynamics in high-energy proton-nucleus collisions, Phys. Rev. C* **88** (2013) 014903 [1304.3044].

9. M.-A. Sanchis-Lozano and E. Sarkisyan-Grinbaum, *A correlated-cluster model and the ridge phenomenon in hadron–hadron collisions, Phys. Lett. B* **766** (2017) 170 [1610.06408].

10. M.-A. Sanchis-Lozano and E. Sarkisyan-Grinbaum, *Ridge effect and three-particle correlations, Phys. Rev. D* **96** (2017) 074012 [1706.05231].

11. J. Noronha, B. Schenke, C. Shen and W. Zhao, *Progress and Challenges in Small Systems*, 1, 2024, 2401.09208.

12. A. Badea, A. Baty, P. Chang, G. M. Innocenti, M. Maggi, C. Mcginn et al., *Measurements of two-particle correlations in e^+e^- collisions at 91 GeV with ALEPH archived data, Phys. Rev. Lett.* **123** (2019) 212002 [1906.00489].

13. BELLE collaboration, *Measurement of Two-Particle Correlations of Hadrons in e^+e^- Collisions at Belle, Phys. Rev. Lett.* **128** (2022) 142005 [2201.01694].

14. Y.-C. Chen et al., *Long-range near-side correlation in e+e− collisions at 183-209 GeV with ALEPH archived data, Phys. Lett. B* **856** (2024) 138957 [2312.05084].

15. M. J. Strassler and K. M. Zurek, *Echoes of a hidden valley at hadron colliders, Phys. Lett. B* **651** (2007) 374 [hep-ph/0604261].

16. R. Pérez-Ramos, M.-A. Sanchis-Lozano and E. K. Sarkisyan-Grinbaum, *Searching for hidden matter with long-range angular correlations at e^+e^- colliders, Phys. Rev. D* **105** (2022) 053001 [2110.05900].

17. T. Sjöstrand, S. Ask, J. R. Christiansen, R. Corke, N. Desai, P. Ilten et al., *An introduction to PYTHIA 8.2, Comput. Phys. Commun.* **191** (2015) 159 [1410.3012].

18. M. Berggren, *SGV 3.0 – a fast detector simulation*, 1203.0217.

19. ILD CONCEPT GROUP collaboration, *International Large Detector: Interim Design Report*, 2003.01116.

20. E. Musumeci, R. Perez-Ramos, A. Irles, I. Corredoira, V. A. Mitsou, E. Sarkisyan-Grinbaum et al., *Two-particle angular correlations in the search for new physics at future e^+e^- colliders*, in *International Workshop on Future Linear Colliders*, 7, 2023, 2307.14734.

21. A. Irles, J. P. Márquez, R. Pöschl, F. Richard, A. Saibel, H. Yamamoto et al., *Probing gauge-Higgs unification models at the ILC with quark–antiquark forward–backward asymmetry at center-of-mass energies above the Z mass, Eur. Phys. J. C* **84** (2024) 537 [2403.09144].

22. P. Bambade et al., *The International Linear Collider: A Global Project*, 1903.01629.

23. M. Bahr et al., *Herwig++ Physics and Manual, Eur. Phys. J. C* **58** (2008) 639 [0803.0883].

24. J. Bellm et al., *Herwig 7.0/Herwig++ 3.0 release note, Eur. Phys. J. C* **76** (2016) 196 [1512.01178].

25. M.-A. Sanchis-Lozano, *Prospects of searching for (un)particles from Hidden Sectors using rapidity correlations in multiparticle production at the LHC, Int. J. Mod. Phys. A* **24** (2009) 4529 [0812.2397].

26. M.-A. Sanchis-Lozano and E. K. Sarkisyan-Grinbaum, *Searching for new physics with three-particle correlations in pp collisions at the LHC, Phys. Lett. B* **781** (2018) 505 [1802.06703].